Length Scales Which Perturb Chain Packing in Amorphous Polymers

Marcin Wachowicz,[†] Justyna Wolak, Hanna Gracz, Edward O. Stejskal, Stefan Jurga,[†] Elizabeth F. McCord,[‡] and Jeffery L. White*

Department of Chemistry, Campus Box 8204, North Carolina State University, Raleigh, North Carolina 27695-8204

Received April 15, 2004; Revised Manuscript Received April 21, 2004

ABSTRACT: Direct spectroscopic probes of individual chain conformation and free volume are used to measure the increasing perturbation in the local glass-transition temperature of one polymer chain with decreasing length scale of mixing in binary polyolefin blends. Solid-state ^{2}H and ^{129}Xe NMR experiments reveal a compositional miscibility window in side-chain concentration for polyisobutylene (PIB)/poly(ethylene-*co*-butene) (PEB) blends. A combination of pulsed-field gradient and chemical shift data for xenon gas absorbed in these polymer blends indicates that the presence of polymer chains within a radius of ∼35 nm of a different chain structure will perturb the intermolecular packing contribution to the total conformational energy of that chain, thereby changing its T_g.

Introduction

Kumar and co-workers have recently published a theoretical paper in which they question the length scales that control dynamics in miscible polymer blends specifically and polymer chains in general.[1] Key considerations in that work include the influence of concentration fluctuations, chain connectivity effects, the size of dynamic heterogeneities or cooperatively rearranging regions, and their temperature dependencies. As evidenced by the large number of recent publications in this general area, these topics are relevant to structure−property relationships in both polymers and inorganic glasses,[2−5] the glass transition length scale,[6−11] the glass transition time scale,[12] and structure relaxation.[13−15] While much of the recent published work has attempted to discern the size or length scale of cooperative motions giving rise to the glass transition, we feel an equally important question for blends of amorphous molecules has to do with what length scale of mixing in a binary mixture is required to change the glass transition characteristics (temperature or time scale) of either component relative to their pure states. Stated differently, one could ask what minimum length scale of concentration fluctuation (or domain size) is required to render all molecules in that region "dynamically perturbed" relative to those same molecules in their pure, bulk environment. The ramifications of this issue are clear for the physical properties of binary polymer blends but are also relevant to the general behavior of polymer interfaces, surfaces, and thin films.

In this contribution, we address the question of length scales experimentally using local spectroscopic probes of polymer chain dynamics and free volume in binary blends of nonassociating polyolefins. Solid-state NMR experiments reveal that different perturbations of the chain-level T_g take place in blends of polyisobutylene (PIB) and poly(ethylene-*co*-1-butene) (PEB), in which the 1-butene comonomer concentration is varied among the blends. Specifically, we monitor the change in local chain dynamics of PIB as the length scale of mixing with PEB changes in the blends. A combination of static ^{2}H (a noninvasive, direct probe of polymer chain dynamics) and ^{129}Xe (a noninvasive, direct probe of local chain packing) NMR experiments, as well as ^{129}Xe pulsed-field gradient diffusion (PFG) NMR, in these solid polymer blends reveals that concentration fluctuations of 60−70 nm (several times R_g) lead to measurable changes in the dynamics of chains included in those regions, relative to their pure bulk dynamics.

Experimental Section

Copolymers of hydrogenated/perdeuterated polyisobutylene were prepared by cationic polymerization of isobutylene monomers. Copolymers of perdeuterated monomers and their hydrogenated analogues are referenced as follows: 80%-PIB-d_8 (M_n = 466 000) copolymer denotes 80% perdeuterated monomers, and 20%-PIB-d_8 (M_n = 353 000) copolymer indicates 20% perdeuteration. Commercial PIB (M_w = 1 000 000) obtained from ExxonMobil Chemical was used for the xenon experiments. The PEB-66 (M_w = 114 000) is the same polymer previously referenced as HPB66 by Graessley and co-workers and is a monodisperse ethylene−butene copolymer obtained by anionic polymerization of butadiene, followed by hydrogenation.[16−18] The degree to which the diene polymerizes 1,2 vs 1,4 addition determines the butene and ethylene concentrations, respectively, as has been extensively discussed in previous papers.[19] The PEB-23 sample is a commerical ethylene−butene copolymer made via metallocene polymerization (M_w = 79 000) and sold as Exact 4041 by ExxonMobil. The 50:50 wt % blends were prepared from dissolution in toluene for 24−48 h, followed by solvent evaporation, and then vacuum-drying to 10^{-2} Torr for 4 days or longer. Thermal analysis of each polymer by DSC revealed the following T_g's: PIB = −68 °C; PEB-66 = −52 °C; PEB-23 = −39 °C; PIB/PEB-66 blend = broad, poorly resolved transition at ca. −61 °C; PIB/PEB-23 blend = two well-resolved transitions at −68 and −39 °C.

All ^{2}H NMR measurements were performed on a Bruker CXP spectrometer operating at a magnetic field strength of 4.7 T, corresponding to 30.7 MHz deuteron resonance frequency. The spectra were recorded using the quadrupole-echo pulse sequence $[(\pi/2)_x-\tau_1-(\pi/2)_y-\tau_2-\text{acq}]$ with a typical pulse width of 3.0 μs. Consequently, pure perdeuterated PIB spectra required 512 scans while the blends required up to 4000 scans to obtain spectra of sufficient sensitivity. The temperature

[†] Department of Macromolecular Physics, Institute of Physics, Adam Mickiewicz University, ul. Umultowska 85, 61−614 Poznan, Poland.

[‡] DuPont Central Research and Development, Experimental Station, Wilmington, DE.

* To whom all correspondence should be addressed: e-mail Jeff_L_White@ncsu.edu.

10.1021/ma049263u CCC: $27.50
Published on Web 05/21/2004

dependence of T_2^{QE} and T_1 relaxation times was measured using the quadrupolar echo (as mentioned above) and inversion−recovery with quadrupole echo detection [$(\pi)_x-\tau_1-(\pi/2)_x-\tau-(\pi/2)_y-\tau-$acq] sequences, respectively.

Weblab version 4.1, an interactive Web-based program, was used for deuteron line shape simulations of the four-site exchange model.[20] The program can be used to calculate quadrupolar echo spectra of $I = 1$ spin system under the influence of molecular motions. Weblab offers ^{2}H NMR one-dimensional theoretical spectrum calculations, but it is limited to discrete jumps on a single cone or the *n*-state jump model. The simulation input parameters consisted of angles, site populations, and reorientation rates while considering two types of motion including fast methyl rotation and trans−gauche isomerization. Simulations were repeated until satisfactory correlation was accomplished between the experimental and the simulated spectra.

^{129}Xe single-pulse NMR experiments were performed on a Bruker AVANCE 500 MHz spectrometer with an Oxford narrow bore magnet. A 10 mm probe (BB500-10EB, Nalorac Cryogenic Corp.) was used for all measurements, and all spectra were acquired at 298 K (with the line from free xenon gas serving as the internal standard at 0 ppm). The instrumental parameters for acquisition of the ^{129}Xe NMR spectra are as follows: spectrometer frequency = 138.365 MHz; spectral width = 83 333 Hz (equivalent to 602 ppm); number of data points = 16K; relaxation delay = 2 s; acquisition time = 0.098 s; pulse width = 16 μs (tip angle = 60°); number of transients > 1K. A thick-walled, valved NMR tube from New Era Enterprises (Part no. NE-CAV5-M-133) was used in conjuction with a Swagelok adapter (Part no. 2-TA-1-OR) to transfer gas from a pressurized line ($^1/_4$ in. stainless steel tubing) to the sample. The tube allows for pressure-controlled experiments by its precise Teflon plug with a Viton O-ring seal. A Delrin adapter was made to attach the NMR tube to the xenon line. To ensure that no pressure blow-out would occur and in order to give more physical control over the sealing method, a Teflon connection was made and connected the sleeve of the NMR tube to the adapter. This sample preparation arrangement is attractive relative to previously published custom designs since all components may be obtained commercially. Typically, 120 psig (equivalent to 9.3 bar, total pressure) of xenon was used; equilibration was almost instantaneous.

The ^{129}Xe diffusion NMR results were obtained on a Varian 400 MHz Inova wide-bore NMR spectrometer with a high gradient strength (up to 1000 G/cm) variable temperature double-coil DOTY diffusion probe equipped with water-cooled gradients. Experiments were run at 30.2 °C using air-cooling. Temperature was calibrated using a thermocouple centered axially in a 5 mm NMR tube at the center of the receiver coil position under normal air-flow conditions. The standard Varian pulse sequence was modified to use trapezoidal-shaped diffusion gradient pulses. The console was equipped with a Performa 3 amplifier whose output was connected to a Techron high-power amplifier for the gradients. Experiments were run using acquisition times of 0.64 s, a recycle delay time of 3 or 5 s, a 14.75 μs 90° pulse, a spectral width of 38.7 kHz, 800 or more transients averaged per increment, analogue filters, and eight increments with diffusion gradients ranging from 50 to 950 g/cm. The optimal gradient pulse length was 4 ms, and the diffusion delay was 50 ms; no differences were observed using a 20 ms delay. Data were processed using line broadening of 40 Hz and zero filling to 128K. We used a monoexponential fit to analyze the data with a weighting function of the inverse square root of the peak intensity. Our data processing force fits to a single exponential even if the species exists in multiple environments, and the raw data are a sum of several different exponential decays.

Results and Discussion

^{2}H NMR Data. In Figure 1, a stack plot of ^{2}H NMR quadrupole echo spectra of 80%-PIB-d_8 is shown as a function of temperature, ranging from 210 to 294 K. At the lowest temperature, Figure 1 shows an overlapping Pake pattern spectrum composed of CD_2 and CD_3 signals. The signals can be assigned to CD_2 and CD_3 by relative amplitudes ($^2/_8$ and $^6/_8$) and different quadrupolar splittings (128 and 39 kHz), respectively.[21] Because of the large 128 kHz splitting, the CD_2 signal collapses beneath the CD_3 signal at higher temperatures and becomes observable only indirectly. At 210 K, the CD_3 group has an anisotropically averaged Pake pattern with a 39 kHz splitting due to rapid rotation along C_3 at a rate greater than the quadrupolar coupling interaction. In order for additional narrowing of the CD_3 signal to take place above 210 K, an additional source of motion that reorients the bond vector between the methyl and the quaternary carbon is required. Since the CD_3 group is directly attached to the quaternary carbon, it acts as a specific probe of the chain backbone conformational dynamics. Further narrowing takes place with increasing temperature due to the slower reorientations of the chain via trans−gauche conformational isomerization. The Pake pattern collapses into a single line with no splitting at 265 K. This coalescence point is followed by further reduction in the line width to yield a simple Lorentzian line shape at room temperature.

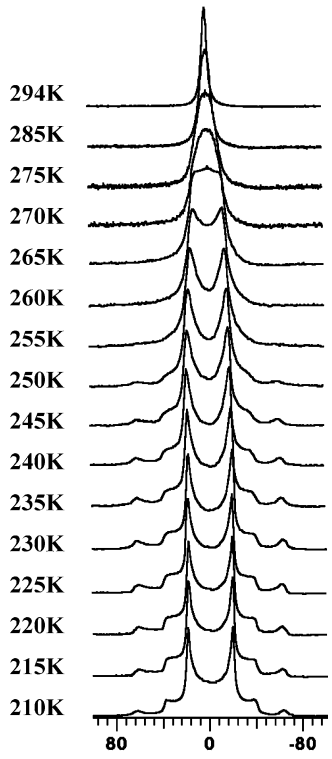

Figure 1. Static ^{2}H NMR spectra for 80%-PIB-d_8 vs temperature, showing a glass transition on the ^{2}H NMR time scale at ≈265 K.

Figure 2 illustrates the unique line shape coalescence point for the three samples vs temperature. The pure 20%-PIB-d_8 sample coalesces at 265 K (Figure 2c), while PIB/PEB-66 (Figure 2a) and PIB/PEB-23 (Figure 2b) coalesce at 255 and 260 K, respectively. The variations in CD_3 line shape for the PIB chains in the respective samples reflect the different frequencies of PIB chain reorientation in each environment. The Pake pattern for the PIB/PEB-66 blend exhibits an NMR glass transition at 255 K while PIB/PEB-23 blend does so at 260 K. Clearly, the PIB chain motional frequencies are perturbed more in the PIB/PEB-66 blend (containing 49

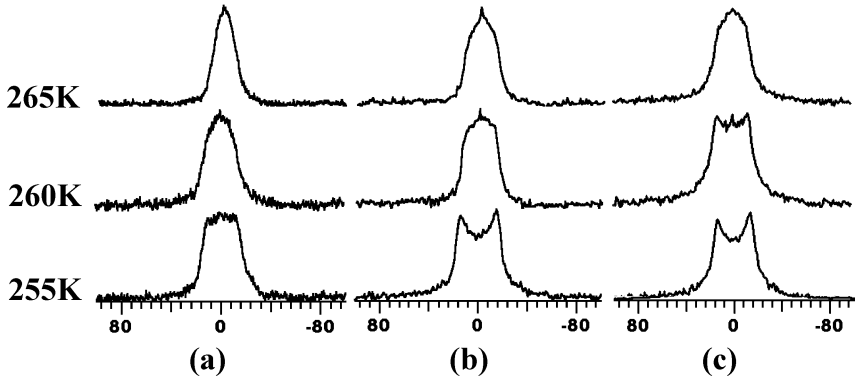

Figure 2. Comparison of static ^{2}H NMR spectra over the NMR T_g range for 20%-PIB-d_8 chains in **(a)** a blend with PEB-66, **(b)** a blend with PEB23, and **(c)** bulk, i.e., pure 20%-PIB-d_8. Note the difference in the spectral coalescence points in both **(a)** and **(b)**, relative to **(c)**, which is even more clear by comparing the line shapes across the second row.

mol % butene) than in the PIB/PEB-23 blend (containing 13% butene). Further inspection of the line width and line shape at 265 K, the pure 20% PIB-d_8 coalescence temperature, indicates that the PIB/PEB-66 line shape is already much more averaged than that of PIB/PEB-23. Clearly, PIB chains in both blends exhibit increased conformational mobility relative to the bulk PIB as a result changing the particular line shape coalescence points of PIB/PEB-23 and PIB/PEB-66 by −5 and −8 deg, respectively. We were particularly surprised to see the −5 K shift for the PIB/PEB-23 blend, since the DSC thermogram shows two distinct, well-resolved T_g's (not shown).

^{2}H Line Shape Simulations. Deuterium spectra simulations were used to extract models of the PIB chain dynamics in the pure PIB and in the two blends. Reasons for restricting the simulations to the CD_3 group and excluding the CD_2 group will be discussed later. Using the simulation program Weblab,[20] two main types of molecular reorientations were included in the CD_3 spectra simulations: fast methyl group rotation and trans−gauche backbone isomerization. Fast methyl rotation reduces the quadrupolar splitting by a factor of 3 while the slower trans−gauche chain isomerization leads to further averaging and, finally, to the collapse of the quadrupolar splitting. The trans−gauche isomerization is frozen at temperatures below ∼230 K, whereas the methyl rotation is still fast on that time scale. This is confirmed by the low temperature spectra in Figures 1 and 2, which exhibit the motionally narrowed splitting of ∼39 kHz.[21] The value is slightly smaller than the 42 kHz theoretical value. This splitting is reduced by a factor of 3 with respect to the value observed for the spectrum of static methyl groups. In the case of methylene groups, once the chain trans−gauche isomerization is frozen there are no other mechanisms that could average the quadrupolar interaction, and consequently a static powder type spectrum of 128 kHz is observed.

Different *n*-site jump models were considered for the trans−gauche isomerization. Ultimately, a four-site exchange model was chosen, with the flip angle equal to 90° and the cone angle equal to the "magic angle" $\theta = 54.74°$. The possible jumps in the four-site exchange model are based on the jumps described by the three-site model (flip angle $\Phi = 120°$, cone angle $\Theta = 70.5°$), except they are observed from a coordinate system that is tilted by an angle of 54.74°.

Figure 3 illustrates two chain segments used for the simulations, showing the all-trans (a) with two methyl groups marked as "A" and "B" switching to a gauche (+ or −) (b) conformation on the top left and right, respectively. The bottom schematic denotes the conformational dynamics model used in the motionally averaged CD_3 powder simulations, with the circle showing the different sites occupied with either methylene or methyl groups in the trans (a) and gauche (b) states.

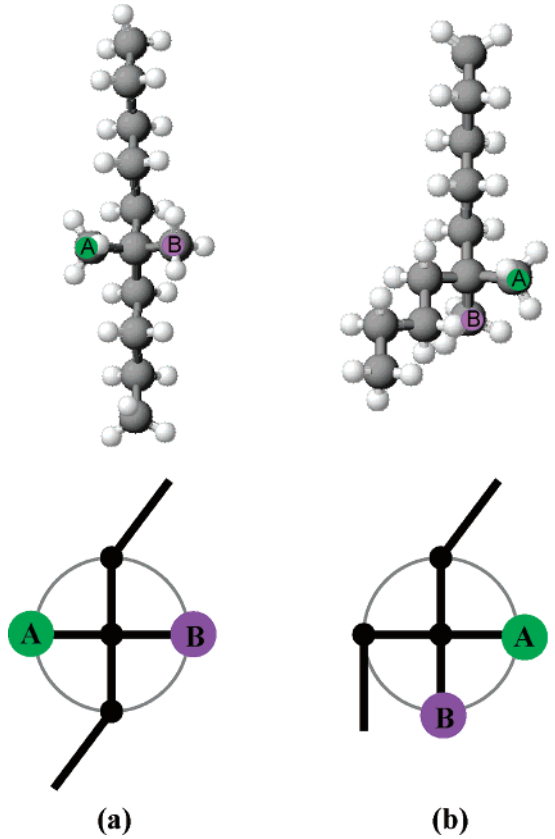

Figure 3. Top schematic shows a simulated conformer of an **(a)** all-trans chain segment with introduction of a single trans−gauche (gauche$^+$ or gauche$^-$) exchange event in **(b)**. Bottom schematic shows conformational dynamics model used to simulate the motionally averaged CD_3 powder patterns. Individual methyl groups are denoted as "A" and "B".

The simulation input parameters included the angles (defining the site orientation involved in a motion), site populations (occupancy probabilities), and reorientation rates (exchange rates among sites). The site probabilities were defined as follows: p_1 for $\Phi = -135°$, p_2 for $\Phi = -45°$, p_3 for $\Phi = 45°$, p_4 for $\Phi = 135°$. These probabilities determine the exchange rates among different sites, which are contained in the exchange matrix.

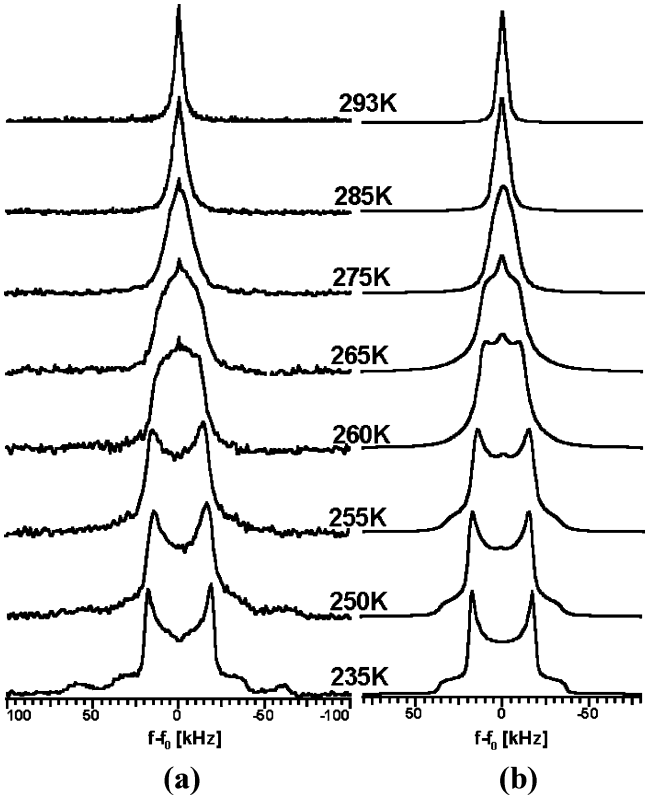

Figure 4. Comparison of **(**a**)** experimental and **(**b**)** simulated variable-temperature ^{2}H spectra for the 20% PIB-d_8 blended with PEB-23.

A limitation of the Weblab model is that the exchange rates between sites "1" and "3" (trans → trans), as well as between "2" and "4" (gauche$^+$ → gauche$^-$), were zero ($v_{13} = v_{31} = v_{24} = v_{42} = 0$). The sum of site probabilities $p_1 + p_3$ corresponded to the total trans conformation probability, while $p_2 + p_4$ corresponded to the total gauche conformation probability. An increased "gauche" site probability results from higher frequency of trans → gauche jumps, and similarly the increased trans probability results from the fact that gauche → trans reorientation dominates over the inverse process. Simulations showed the expected increase in gauche conformer population with increasing temperature (not shown).

Theoretical spectra were calculated starting with the room temperature experimental line shapes and then varying the relative trans and gauche conformational contributions together with the reorientation rates. Figure 4 demonstrates the excellent agreement between the experimental (Figure 4a) and simulated (Figure 4b) spectra for PIB/PEB-23. To gain correlation at lower temperatures, the average reorientation rate was decreased, and site probabilities were systematically changed, causing the expected decrease of gauche chain conformational contributions. Equal probabilities for gauche$^+$ and gauche$^-$ conformations were assumed ($p_2 = p_4$). The four-site model has two sites that correspond to the trans conformation (p_1, p_3) by which one can achieve a jump rate distribution that will vanish in the limit of $p_1 = p_3$ or when one of these probabilities approaches zero.

All three samples (PIB, PIB/PEB-66, and PIB/PEB-23) were accurately simulated using the four-jump model, which demonstrates that the PIB chain dynamics are the same in all samples. The only difference is that

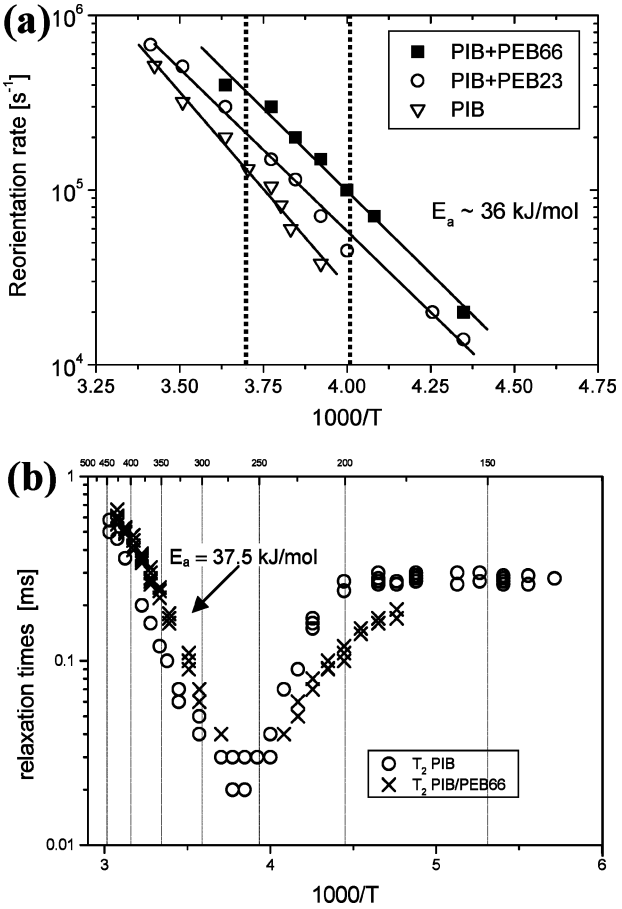

Figure 5. **(**a**)** Arrhenius plot of chain reorientation rates obtained via simulation of the experimental static ^{2}H line shapes using the four-site model described in the text for 20% PIB-d_8 chains in each of the indicated environments. The dotted lines indicate the region near line shape collapse. **(b)** Relaxation rate data vs temperature for ^{2}H T_2 experiments. Note that the same activation energy is obtained via line shape simulation **(**a**)** and in the linear region of the T_2 curve **(**b**)**.

the motional frequency is increased at any temperature in the blends relative to the pure 20%-PIB-d_8. As mentioned before, the conformational dynamics of PIB are perturbed in the PIB/PEB-66 blend more than those in PIB/PEB-23, or in other words, the effective NMR T_g is reduced further. Figure 5a shows the reorientation rate obtained from the four-site jump model as a function of temperature for the pure 20%-PIB-d_8, 20%-PIB-d_8/PEB-23, and 20%-PIB-d_8/PEB-66. The slopes of the three systems indicate an isomerization activation energy equal to 36 kJ/mol. Additonally, the graph signifies intermediate behavior for the PIB/PEB-23 blend relative to the pure 20%-PIB-d_8 and the PIB/PEB-66. The activation energy obtained from the line shape simulations can be compared with the model-free relaxation experiments, e.g., T_2^{QE} as a function of temperature. From the graph in Figure 5b, the right and upward shift in the T_2^{QE} upon blending PIB with PEB-66 is evident, at the same time also revealing an activation energy equal to 37.5 kJ/mol. The direct link between the simulated and experimental data is clearly demonstrated by the matching activation energies acquired by two different methods, one of which is independent of any assumptions or physical model.

Using the direct connection between the simulated and experimental data, the justification for neglecting the CD_2 contribution to the theoretical spectrum calcu-

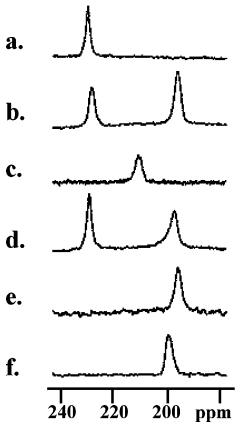

Figure 6. Static ^{129}Xe NMR spectra for xenon gas absorbed in **(**a**)** pure PIB vs blends with decreasing 1-butene comonomer amounts: **(**b**)** 50:50 PIB/PEB-97 blend; **(**c**)** 50:50 PIB/PEB-66 blend; **(**d**)** 50:50 PIB/PEB-23 blend; **(**e**)** pure PEB-97; **(**f**)** pure isotactic poly-1-butene. The free xenon peak at 0 ppm is not shown for clarity, and lower sample masses were used in (c) and (e).

lations for the PIB molecule is reasonable. As seen in Figure 1 and the PIB/PEB-23 stack plot in Figure 4a, the CD_2 contribution was resolved at temperatures below ~230 K as a broad component with static splitting equal to ~128 kHz. Because of the deuteron ratio in the monomer ($2CD_3$:CD_2 or 3:1), the integrated intensity of the CD_2 group is ~3 times smaller than the intensity of a CD_3 group spectrum. Furthermore, the sensitivity of ^{2}H NMR blend spectra was decreased by the lower degree of perdeuterated PIB monomers even with increased acquisitions. The conformational interchange along the backbone will act to narrow the CD_3 and CD_2 line shapes at the same rate vs temperature, i.e., with the same activation energy. Therefore, the relative comparison of activation energies between the three samples should not be complicated by the fact that the CD_2 component is not explicitly treated in the simulations.

Basis for Tetrahedral Jump Model Assignment. In the absence of additional experimental information, one cannot unequivocally assign the observed changes in the ^{2}H line shapes to 120° internal rotations associated with rapid tetrahedral jumps vs small-angle librational motions. English and co-workers have previously discussed the quantitative relationships between motional time scales, echo times, motional models, and the one-dimensional ^{2}H line shape.[22,23] On the basis of our previously published two-dimensional solid-state ^{13}C exchange experiments for these polymers and their blends, it is clear that individual PIB chain segments are undergoing tetrahedral jumps at a rate of 65−75 kHz over the temperature range associated with line shape collapse in Figure 2.[12,24] From this work we assigned the jump model to the ^{2}H line shape simulations and note that the refocusing efficiency of the integrated line shape intensity was found to decrease by almost a factor of 2 when the total echo delay time was increased from 20 to 80 μs, as expected from ref 23.

^{129}Xe NMR. ^{129}Xe NMR is a sensitive and nondestructive technique capable of probing the length scale of mixing, or domain size in the two blends.[25,26] Xenon's large, highly polarizable electron density, but small van der Waals radius of 2.2 Å, makes it an appealing tool for probing slight changes in the electronic environment of blends.[27] Figure 6 demonstrates that simple one-pulse Xe NMR experiments are remarkably sensitive to different polyolefin environments.[26] In Figure 6, results are presented for ^{129}Xe chemical shift in pure PIB, pure poly-1-butene (P1B), and several blends. In contrast to all other blends of PIB with PEB or P1B, the PIB/PEB-66 blend (Figure 6c) shows only one resonance, indicating that the xenon molecule is diffusing in a homogeneous molecular environment (as defined by the diffusion coefficient of xenon in that blend). For comparison, the PIB/PEB-23 blend shows two clearly resolved resonances (Figure 6d), corresponding very closely with the two pure component PIB and PEB-23 shifts. Here, xenon gas diffuses between two dissimilar surroundings, which match the two constituents, indicative of a much larger length scale of mixing, or domain size, relative to PIB/PEB-66 (vide infra). A similar microphase-

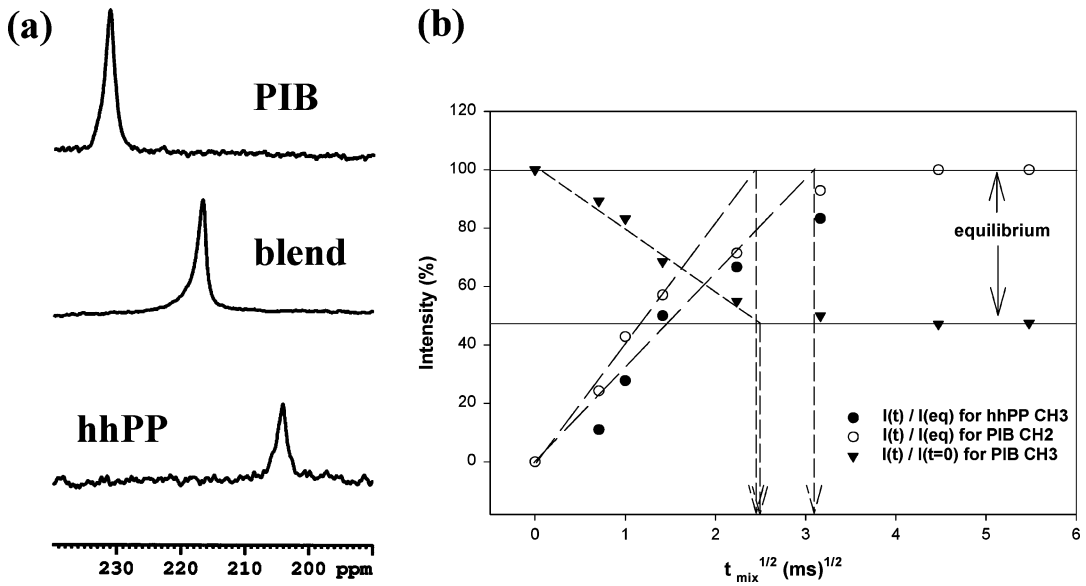

Figure 7. Comparison of two noninvasive experimental methods of miscibility for a polyolefin blend: **(**a**)** static ^{129}Xe spectra of a PIB/hhPP blends vs its pure components; **(**b**)** ^{1}H solid-state spin diffusion data for the same blend as in (a). Note that the slopes of all increasing and decreasing curves in (b) are of similar absolute magnitude, indicating that polarization transfer between PIB and hhPP chains occurs with a time scale similar to spin-diffusion within PIB chains, proving intimate mixing.[29,30]

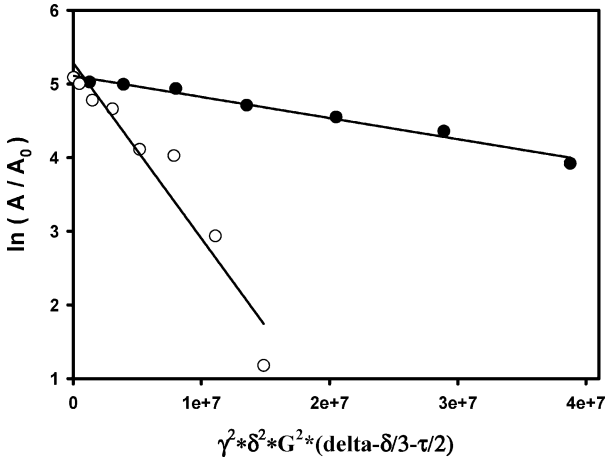

Figure 8. ^{129}Xe PFG experimental results for pure PIB (●) and PIB/PEB-66 (○), yielding diffusion coefficients of 2.9 × 10^{-8} and 2.0 × 10^{-7}cm^2/s, respectively.

separated result is obtained for a blend of PIB/PEB-97 (Figure 6b). Figure 6b−d reveals a compositional miscibility window in 1-butene concentration for blends of PEB with PIB.

The fact that the chemical homogeneity of a miscible binary blend is accurately reflected by a single Xe signal is illustrated in Figure 7 for a blend of PIB with hhPP (head-to-head polypropylene). We would have preferred a direct measurement of mixing via ^{1}H spin diffusion in the PIB/PEB blends used in this study.[28] Unfortunately, the differences in overall chain dynamics, and ^{1}H chemical shifts in the solid state, for PIB vs PEB were insufficient to allow spin-diffusion measurements. Therefore, we did a comparative analysis on a polyolefin blend where both Xe NMR and ^{1}H spin-diffusion experiments were possible. In Figure 7, the Xe chemical shift results are compared to ^{1}H spin-diffusion NMR data for the same sample of PIB/hhPP, a blend pair which is known to be miscible.[29] Indeed, this blend is intimately mixed at the chain level (length scale of 2.5 nm which is $\ll R_g$), as shown by the spin-diffusion plot in Figure 7, the analysis of which has been previously published.[29,30] Figure 7 demonstrates that if intimate chain mixing occurs in a polymer blend, a single Xe chemical shift will be observed. However, the presence of a single Xe line does not prove intimate mixing at the chain level; it shows only that the blend is homogeneous on a length scale defined by the Xe diffusion coefficient.

To quantitatively analyze the Xe chemical shift data from Figure 6 in terms of average domain size or concentration length scale in the PIB/PEB blends, ^{129}Xe pulsed-field gradient (PFG) spin-echo experiments were used to measure the physical diffusion coefficient of Xe in the samples.[31−34] In these experiments a magnetic field gradient is used to spatially encode the sample along the *z*-axis. A delay period is then introduced during which the molecules can diffuse out of place with respect to the *z* spatial encoding. Following the delay period, a reverse magnetic field gradient is applied which refocuses the magnetization and produces an echo signal for the molecules which have not diffused out of place. Echo signal measurements as a function of gradient strength consequently determine the specific diffusion coefficients as seen in Figure 8 for PIB and PIB/PEB-66 samples.

A least-squares analysis of the PFG data according to eq 1 with I (echo intensity), γ (magnetogyric rato), δ (gradient pulse length), G (gradient strength), D (diffusion coefficient), τ (midpoint separation time of bipolar gradient pulses), and Δ (diffusion delay) allows the diffusion coefficients for PIB and PIB/PEB-66 to be determined as 2.9 × 10^{-8} and 2.0 × 10^{-7} cm^2/s, respectively.

$$I = I_0 \exp[-\gamma^2\delta^2G^2D(\Delta - \delta/3 - \tau/2)] \qquad (1)$$

Almost a factor of 7 difference exists for the diffusion coefficients of xenon in pure PIB and PIB/PEB-66, demonstrating that upon blending the PIB chains adopt a new, less confined packing structure relative to the bulk PIB. Using the diffusion coefficient for the PIB/PEB-66 blend together with the chemical shift difference of the two constituents (4841 Hz), the length scale of mixing in the PIB/PEB-23 blend is calculated to be >70 nm, while that for the PIB/PEB-66 blend is <70 nm. Figure 9 depicts the organization of polymer chains between PIB-rich and PEB-rich regions.

Conclusions

Chain packing in blends of amorphous, nonassociating polymers has been shown to be influenced by length scales of mixing even larger than 70 nm, a value which is significantly greater than the dimensions of individual polymer chains in their bulk states (<10 nm). Conformational dynamics of individual polymer chains at the glass transition are measurably and reproducibly per-

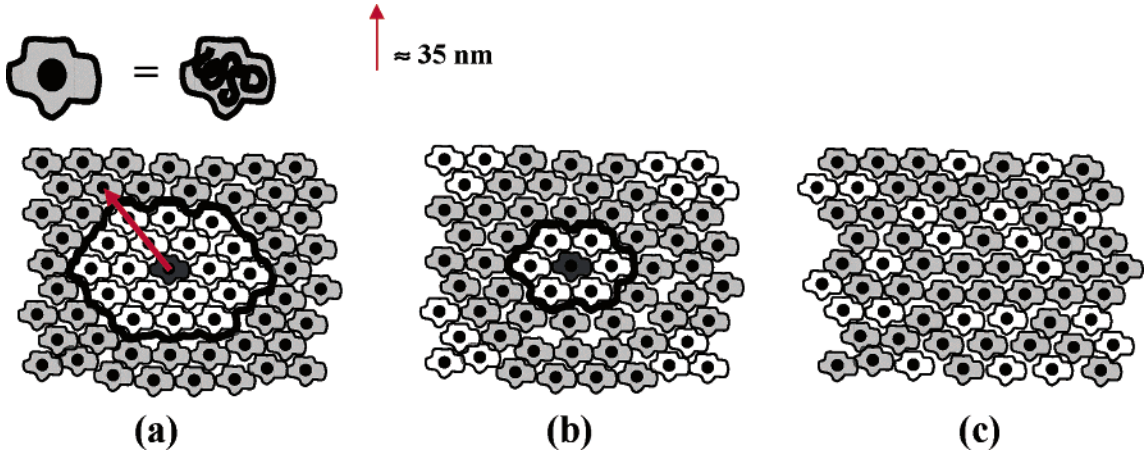

Figure 9. Schematic of mixing length scales derived from Xe NMR data in **(a)** the PIB/PEB-23 blend. For the PIB/PEB-66 blend, either **(b)** or **(c)** is possible representations, since the average domain size is <70 nm for each.

turbed in blends of polyisobutylene and poly(ethylene-*co*-butene) that are microphase separated on these length scales, although less so than similar blends with more intimately mixed chains. A miscibility window in 1-butene composition was found for blends of PIB/PEB; blends containing PEB with 49 mol % 1-butene comonomer were more intimately mixed with PIB than those having 13 or 90 mol % 1-butene comonomer. Our experiments define an alternative view of the "T_g length scale", in that they directly reveal limits on how close one type of polymer chain has to get to another in order to alter its conformational energy surface, i.e., the interchain contribution to its total conformational energy. Our results on binary blends suggest that a gradient of polymer chain dynamics, and T_g's, exists at surfaces or interfaces, with the thickness of that gradient equal to several times the polymer radius of gyration.

Acknowledgment. This work was supported by the National Science Foundation Grant DMR-0137968 and is gratefully acknowledged. Additional support from a DuPont Science and Engineering Award is also acknowledged (J.L.W.). The National Research Council Eastern European Twinning program provided travel support for J.L.W., J.E.W., M.W., and S.J. The authors thank Dr. Tim Shaffer of Exxon Research and Engineering for synthesis of the various deuterated polyisobutylenes. We are grateful to Dr. David J. Lohse of Exxon Research and Engineering for providing the ethylene−butene copolymers used in this work.

References and Notes

(1) Kant, R.; Kumar, S. K.; Colby, R. H. *Macromolecules* **2003**, *36*, 10087.
(2) Lodge, T. P.; McLeish, T. C. B. *Macromolecules* **2000**, *33*, 5278.
(3) Huang, D.; Simon, S. L.; McKenna, G. B. *J. Chem. Phys.* **2003**, *119*, 3590.
(4) Corezzi, S.; Floretto, D.; Rolla, P. *Nature (London)* **2002**, *420*, 653.
(5) Jones, R. A. L. *Nature (London)* **2003**, *2*, 645.
(6) Tracht, U.; Wilhelm, M.; Heuer, A.; Feng, H.; Schmidt-Rohr, K.; Spiess, H. W. *Phys. Rev. Lett.* **1998**, *81*, 2727.
(7) Hempel, E.; Hempel, G.; Hensel, A.; Schick, C.; Donth, E. *J. Phys. Chem. B* **2000**, *104*, 2460.
(8) Donth, E. *J. Polym. Sci., Polym. Phys.* **1996**, *34*, 2881.
(9) Bennenmann, C.; Donati, C.; Baschnagel, J.; Glotzer, S. C. *Nature (London)* **1999**, *399*, 246.
(10) Ediger, M. D.; Skinner, J. L. *Science* **2001**, *292*, 233.
(11) Deschenes, L. A.; Vanden Bout, D. A. *Science* **2001**, *292*, 255.
(12) Wolak, J. E.; Jia, X.; White, J. L. *J. Am. Chem. Soc.* **2003**, *125*, 13660.
(13) Heuer, A.; Wilhelm, M.; Zimmermann, H.; Spiess, H. W. *Phys. Rev. Lett.* **1995**, *75*, 2851.
(14) Ediger, M. D. *J. Phys. Chem. B* **1999**, *103*, 4177.
(15) Tanaka, H. *J. Chem. Phys.* **1996**, *105*, 9375.
(16) Krishnamoorti, R.; Graessley, W. W.; Fetters, L. J.; Garner, R. T.; Lohse, D. J. *Macromolecules* **1995**, *28*, 1252.
(17) Krishnamoorti, R.; Graessley, W. W.; Dee, G. T.; Walsh, D. J.; Fetter, L. J.; Lohse, D. J. *Macromolecules* **1996**, *29*, 367.
(18) Graessley, W. W.; Krishnamoorti, R.; Reichart, G. C.; Balsara, N. P.; Fetter, L. J.; Lohse, D. J. *Macromolecules* **1995**, *28*, 1260.
(19) Balsara, N. P.; Fetters L. J.; Hadjichristdis, N.; Lohse, D. J.; Han, C. C.; Graessley, W. W.; Krishnamoorti, R. *Macromolecules* **1992**, *25*, 6137.
(20) Macho, V.; Brombacher, L.; Spiess, H. W. *The NMR-WEBLAB: an Internet Approach to NMR Lineshape Analysis*, Appl. Magn. Reson. 20,405, 2001.
(21) Jelinski, L. W. In *High-Resolution NMR Spectroscopy of Synthetic Polymers in Bulk*; Komoroski, R. A., Ed.; VCH Publishers: Deerfield Beach, FL, 1986.
(22) Hirschinger, J.; English, A. D. *J. Magn. Reson.* **1989**, *85*, 542.
(23) Schadt, R. J.; Cain, E. J.; English, A. D. *J. Phys. Chem.* **1993**, *97*, 8387.
(24) Wolak, J. E.; Jia, X.; Jurga, S. J.; Gracz, H.; Stejskal, E. O.; White, J. L. *Macromolecules* **2003**, *36*, 4844.
(25) Walton, J. H.; Miller, J. B.; Roland, C. M.; Nagode, J. B. *Macromolecules* **1993**, *26*, 4052.
(26) Schantz, S.; Veeman, W. S. *J. Polym. Sci., Polym. Phys.* **1997**, *35*, 2681.
(27) Bondi, A. *J. Phys. Chem.* **1964**, *68*, 441.
(28) VanderHart, D. L. *Macromol. Chem. Macromol. Symp.* **1990**, *38*, 125. (b) VanderHart, D. L.; McFadden, G. M. *Solid State NMR* **1996**, *7*, 45.
(29) White, J. L.; Lohse, D. J. *Macromolecules* **1999**, *32*, 958.
(30) White, J. L.; Wang, X. *Macromolecules* **2002**, *35*, 3795.
(31) Stejskal, E. O.; Tanner, J. E. *J. Chem. Phys.* **1965**, *42*, 288.
(32) Wu, D.; Chen, A.; Johnson, C. S., Jr. *J. Magn. Reson.* **1995**, *115*, 260.
(33) Johnson, C. S., Jr. *Prog. NMR Spectrosc.* **1999**, *34*, 203.
(34) Junker, F.; Veeman, W. S. *Macromolecules* **1998**, *31*, 7010.

MA049263U